

Article

Preliminary Analysis of Ionospheric Anomalies before Strong Earthquakes in and around Mainland China

Binbin Zhao ^{1,2}, Cai Qian ^{1,2}, Huaizhong Yu ^{3,*}, Jianming Liu ^{1,2}, Nilupaer Maimaitusun ^{1,2}, Chen Yu ³, Xiaotao Zhang ³ and Yuchuan Ma ³

¹ Xinjiang Pamir Intracontinental Subduction National Field Observation and Research Station, Urumqi 830011, China; tszhaobinbin@126.com (B.Z.); charliesqq@163.com (C.Q.); inner369@sina.com (J.L.); nilupar86@163.com (N.M.)

² Earthquake Agency of Xinjiang Uygur Autonomous Region, Urumqi 830011, China

³ China Earthquake Networks Center, Beijing 100045, China; yuchen@seis.ac.cn (C.Y.); zhangxiaotao@seis.ac.cn (X.Z.); mayuchuan@seis.ac.cn (Y.M.)

* Correspondence: yuhz750216@sina.com; Tel.: +86-139-1006-2167

Abstract: The aims of the present study were to use Langmuir Probe payload electron density data and Plasma Analyzer Package payload O⁺ density data from the Zhangheng-1 electromagnetic satellite to statistically analyze anomalies in electron and oxygen ion densities before strong earthquakes ($M_s \geq 6.0$) in western China and its neighboring areas. The goal was to investigate the physical mechanisms underlying electron and oxygen ion generation by evaluating the correlations between such anomalies and the seismic activity before the 6.4-magnitude earthquake in Yangbi, Yunnan, China, on 21 May 2021. Nine (75%) of the twelve earthquakes that occurred during the study period and were not affected by magnetic storms were preceded by anomalous electron or oxygen ion densities of $1.1\text{--}4.5 \times 10^{10}/\text{m}^3$ and $2.8\text{--}6.0 \times 10^{10}/\text{m}^3$, respectively. The anomalies were generally observed within the two weeks preceding the earthquakes and were associated with most strike-slip and thrust earthquakes, which were mainly located on the southeastern and northwestern edges of the Tibetan Plateau—but not normal fault earthquakes. The anomalies were likely the result of acoustic-gravity waves generated by slow vibrations of the Earth's surface reaching the ionosphere, where they cause oscillations in ionospheric electron and ion densities. In addition, the association between ionospheric anomalies and strong earthquakes was confirmed by the observation of other atmospheric anomalies before the Yangbi earthquake.

Keywords: Zhangheng-1 satellite; electron density; ion density; ionospheric perturbation; anomaly mechanism



Citation: Zhao, B.; Qian, C.; Yu, H.; Liu, J.; Maimaitusun, N.; Yu, C.; Zhang, X.; Ma, Y. Preliminary Analysis of Ionospheric Anomalies before Strong Earthquakes in and around Mainland China. *Atmosphere* **2022**, *13*, 410. <https://doi.org/10.3390/atmos13030410>

Academic Editors: Xuemin Zhang and Chieh-Hung Chen

Received: 21 January 2022

Accepted: 28 February 2022

Published: 2 March 2022

Publisher's Note: MDPI stays neutral with regard to jurisdictional claims in published maps and institutional affiliations.



Copyright: © 2022 by the authors. Licensee MDPI, Basel, Switzerland. This article is an open access article distributed under the terms and conditions of the Creative Commons Attribution (CC BY) license (<https://creativecommons.org/licenses/by/4.0/>).

1. Introduction

The development of space exploration technology has promoted the observation of ionospheric anomalies via satellites, which provide a rapid and efficient means for the observation of Earth-based processes, regardless of location or weather. These tools have great potential for facilitating earthquake mechanism research, earthquake monitoring and forecasting, earthquake disaster prevention, and post-earthquake emergency rescue work. The technology also provides great help for short-term earthquake prediction [1,2] and is becoming an important tool for earthquake monitoring and forecasting, as well as for scientific research [3,4].

The Lithosphere–Atmosphere–Ionosphere Coupling (LAIC) is the most common explanation for the ionosphere anomalies caused by the preparation and occurrence of large earthquakes [5]. Recent studies have reported that the ionosphere is unusually sensitive to seismic responses and pre-seismic anomalous information can be extracted from ionospheric perturbations [6–16]. Strong earthquakes may be preceded by anomalous

ionospheric perturbations, with anomaly magnitude increasing with earthquake magnitude [1,17,18]. Most anomalies occur within the 15 days preceding an earthquake and are characterized by simultaneous anomalies across multiple parameters. For example, before the 8.0-magnitude Wenchuan earthquake in 2008, there were drastic changes in electron density, electron temperature, and oxygen ion density near the earthquake epicenter, as well as changes in electromagnetic radiation [17,19,20], and, before the 8.8-magnitude Chilean earthquake in 2010, the 7.2-magnitude earthquake in Yutian, Xinjiang, China in 2008, the 6.9-magnitude earthquake in Gaize, Tibet in 2008, and the 8.6-magnitude earthquake in Sumatra in 2005, simultaneous anomalies in electric field, magnetic field, and several plasma parameters were observed near the earthquake epicenter and may have been related to pre-seismic crustal activity [20–25]. Li et al. (2014) analyzed global moderate-to-strong pre-seismic anomalous ionospheric perturbations and reported that earthquake-related ionospheric perturbations mainly occur one week before an earthquake [1].

The aims of the present study were to use Langmuir Probe (LAP) payload electron density data and Plasma Analyzer Package (PAP) payload O⁺ density data from the Zhangheng-1 electromagnetic satellite to statistically analyze anomalies in electron and oxygen ion densities before strong earthquakes ($M_s \geq 6.0$) in western China and its neighboring areas and to investigate the physical mechanisms underlying electron and oxygen ion generation by evaluating the correlations between such anomalies and the seismic activity before the 6.4-magnitude earthquake in Yangbi, Yunnan, China on 21 May 2021.

2. Materials and Methods

2.1. Satellite and Payload Information

The Zhangheng-1 satellite, which was launched on 2 February 2018, is China's first Seismo-Electromagnetic Satellite and a sun-synchronous orbit satellite with an orbital inclination of 97.4°, flight altitude of 507 km, and observation range of 65° north and south of the equator. The satellite orbits the Earth once every ~94.6 min and can orbit the Earth ~15 times a day, with a revisit period of 5 d. The mean orbital longitude of a revisit period is 4.8°, which corresponds to a distance of ~500 km from the equatorial region, and the orbit of the next revisit period will strictly follow the previous orbit to ensure that the revisit orbit is spatially consistent [26].

The Zhangheng-1 satellite is the first space-based platform in China's three-dimensional seismic observation system and the first satellite in China's geophysical field detection satellite program, the main scientific objectives of which are to acquire and reconstruct the global geomagnetic and ionospheric environments and their dynamic models, to evaluate new methods for short-range earthquake forecasting to develop earthquake theories, and to study space weather processes, as well as Earth's lithosphere–atmosphere–ionosphere coupling mechanisms [27].

The ionospheric observation data of the LAP and PAP payloads were stored in an H5 format for each half orbit (ascending/descending orbit) and are divided into five levels. The Second-level data consist of physical quantity data with orbital parameters that are commonly used in scientific research. The data of this study are taken from the Second-level data observations.

The LAP payload can measure in situ electron density in the range of 5×10^8 to $1 \times 10^{13} / \text{m}^3$, as well as electron temperature, suspension potential, and plasma potential, whereas the PAP payload can detect in situ H⁺ density, He⁺ density, O⁺ density, ion temperature, ion drift velocity, and ion density fluctuations. The LAP payload electron density and PAP payload O⁺ density were used for the present study. There are two operating modes of the satellites, LAP were sampled every 3 s in inspection mode, and the payloads were switched to detailed inspection mode when passing through the seismic zone or any other region of China with sampling every 1.5 s, and PAP were sampled every 1 s [28].

2.2. Anomaly Extraction

The present study used observational data from 1 January 2019 to 9 October 2021, which consisted of electron and O⁺ density data from the LAP and PAP payloads, respectively. Nighttime (i.e., ascending orbit) data were selected, since such data are generally less affected by the sun, and data from days where K_p index ≥ 3 were excluded to remove the possibility of magnetic storm interference. In addition, data from each 5-d period were combined into single files, which were then gridded and plotted using the kriging method.

There were 15 strong ($M_s \geq 6.0$) earthquakes that had occurred in and around the Tibetan Plateau in western mainland China from 1 January 2019 to 9 October 2021, in which 12 earthquakes were included in this study—except three, which were preceded by severe magnetic storm disturbances (Figure 1). The modern tectonic and seismic activity of the Tibetan Plateau is the strongest in China [29] and is associated with subduction of the Indian plate beneath the Eurasian plate, which has formed the modern Himalayan orogenic belt with elevations exceeding 8000 m above sea level. This tectonic zone extends to east- and westward tectonic junctions at Namche Barwa and Nanga Parbat, which turn toward the Burmese arc and Pakistan, respectively. The eastern tectonic junction affects the Sichuan, Yunnan, and Tibet regions of China, and the western tectonic junction affects the Hindu Kush and Pamir regions [29,30]. Most earthquakes of $M_s \geq 6.0$ in mainland China occur in the Tibetan Plateau and its adjacent areas [31].

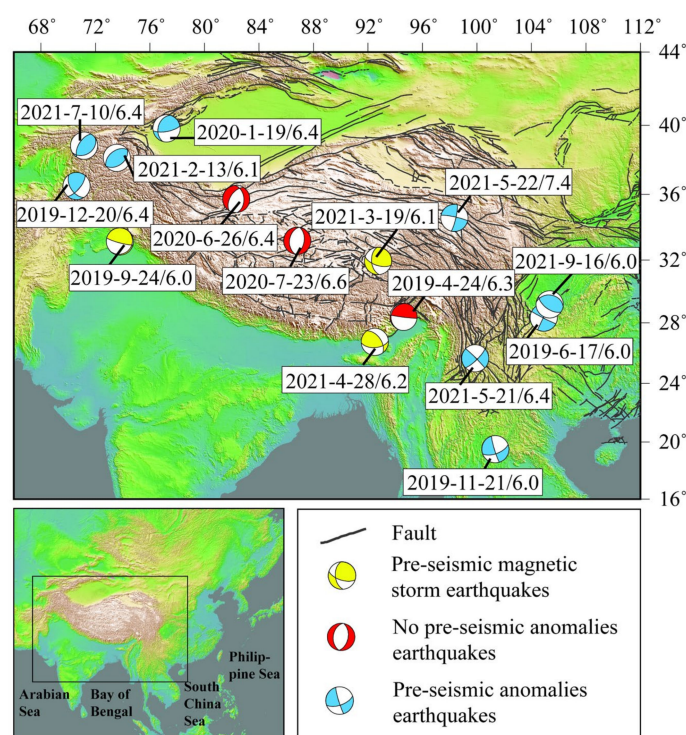


Figure 1. Distribution of earthquake epicenters and pre-seismic ionospheric anomalies in and around western mainland China since 2019.

3. Results and Analysis

3.1. Analysis of Anomalous Characteristics

Previous studies have found that most ionospheric anomalies occur within 15 days before an earthquake. Therefore, the data of the ascending orbit of one month before the earthquake were selected for analysis in this article, in which the data with $K_p \geq 3$ were excluded. The values between adjacent tracks were calculated by using the Kriging interpolation method. In Figures 2 and 3, each graph shows the orbital data for five days and the black parallel lines represent the location where the orbit passes. The spatial scope

of the ionosphere anomalies is 300 km for an earthquake with a magnitude of 6.0–6.9 and 400 km for a $M_s \geq 7.0$ earthquake.

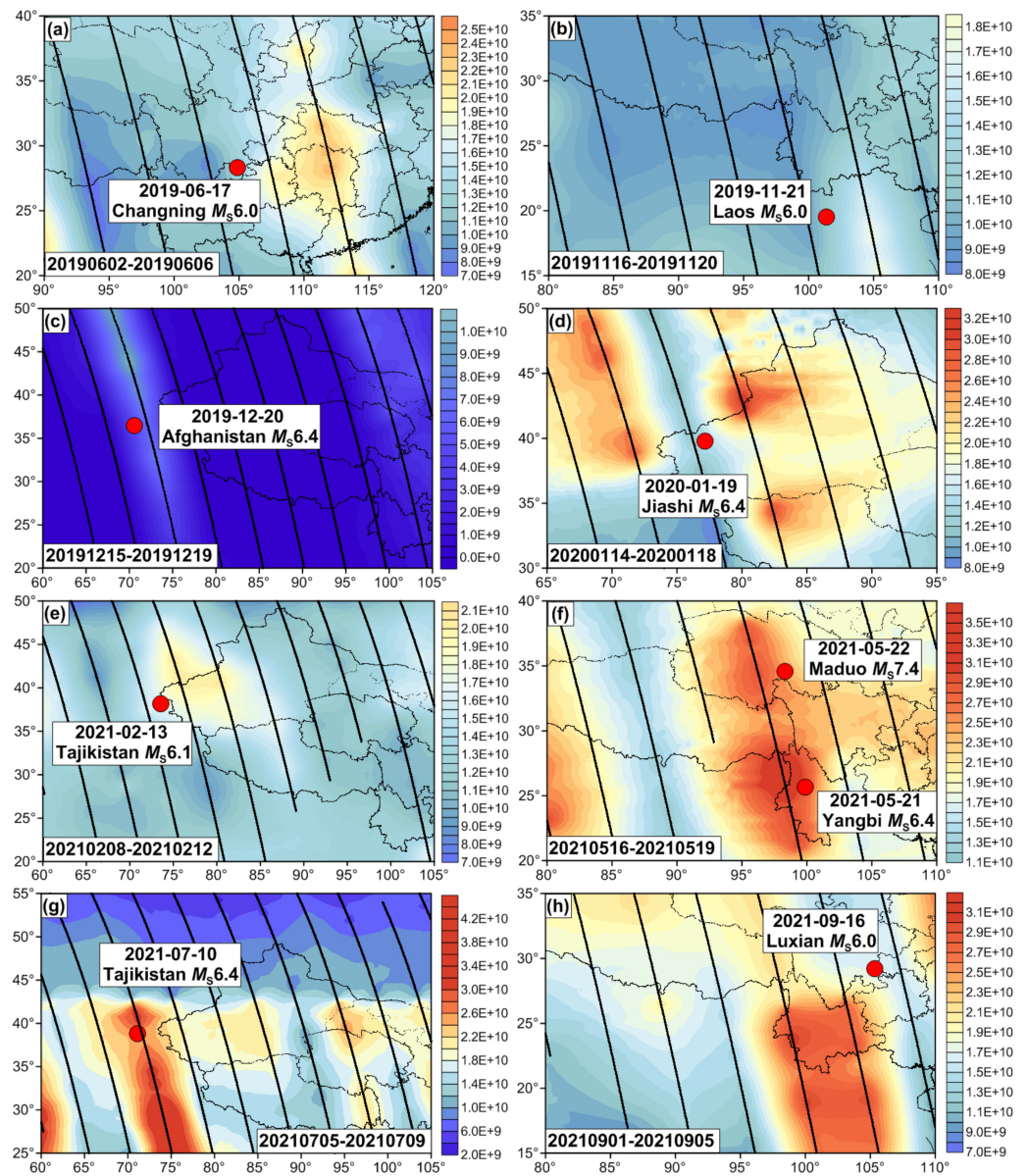


Figure 2. Electron density anomalies observed before strong earthquakes in and around western China. Red circles indicate earthquake epicenters. The maps in (a–e,g,h) are of the M_s 6.0 Changning, M_s 6.0 Laos, M_s 6.4 Afghanistan, M_s 6.4 Jiashi, M_s 6.1 and M_s 6.4 Tajikistan and M_s 6.0 Luxian earthquakes, respectively. (f): the M_s 6.4 Yangbi and M_s 7.4 Maduo earthquakes.

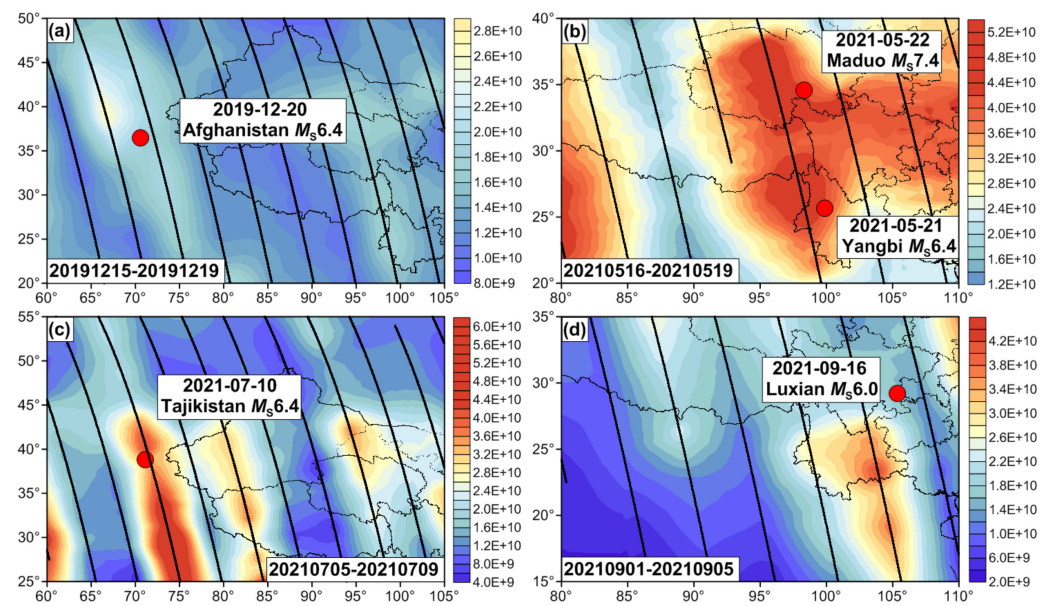


Figure 3. Oxygen ion density anomalies observed before strong earthquakes in and around western China. Red circles indicate earthquakes epicenters. The maps in (a,c,d) are of the M_s 6.4 Afghanistan, M_s 6.4 Tajikistan and M_s 6.0 Luxian earthquakes. (b): the M_s 6.4 Yangbi and M_s 7.4 Maduo earthquakes.

Of the 12 earthquakes included in the present study (Table 1), except for the three earthquakes (3/12) in Motuo, Tibet (M_s 6.3, 24 April 2019); Yutian, Xinjiang (M_s 6.4, 26 June 2020); and Nima, Tibet (M_s 6.6, 23 July 2020), which were not preceded by obvious anomalies in either electron or oxygen ion density, the remaining nine earthquakes (9/12) were preceded by varying degrees of anomalous electron or oxygen ion densities.

Table 1. Statistical information of anomalies before strong earthquakes.

No.	Date DD-MM-YYYY	Location	Longitude/°	Latitude/°	Seismic Magnitude/ M_s	Fault Type	Anomaly Type	Anomaly Time	Greatest Value of Anomaly $\times 10^{10}/m^3$
1	24-04-2019	Medog, Tibet	94.61	28.40	6.3	Thrust			
2	17-06-2019	Changning, Sichuan	104.90	28.34	6.0	Slip	Electron	2 weeks before	2.6
3	21-11-2019	Laos	101.35	19.50	6.0	Slip	Electron	1 week before	1.8
4	20-12-2019	Afghanistan	70.60	36.50	6.4	Slip	Electron Oxygen ion	1 week before 1 week before	1.1 2.8
5	19-01-2020	Jiashi, Xinjiang	77.21	39.83	6.4	Thrust	Electron	1 week before	3.3
6	26-06-2020	Yutian, Xinjiang	82.33	35.73	6.4	Normal			
7	23-07-2020	Nima, Tibet	86.81	33.19	6.6	Normal			
8	13-02-2021	Tajikistan	73.55	38.15	6.1	Thrust	Electron	1 week before	2.1
9	21-05-2021	Yangbi, Yunnan	100.02	25.61	6.4	Slip	Electron Oxygen ion	1 week before 1 week before	3.6 5.2
10	22-05-2021	Maduo, Qinghai	98.34	34.59	7.4	Slip	Electron Oxygen ion	1 week before 1 week before	2.9 5.0
11	10-07-2021	Tajikistan	71.15	38.85	6.4	Thrust	Electron Oxygen ion	1 week before 1 week before	4.5 6.0
12	16-09-2021	Luxian, Sichuan	105.34	29.2	6.0	Thrust	Electron Oxygen ion	2 weeks before 2 weeks before	3.2 4.4

Of the nine earthquakes associated with pre-seismic anomalies, earthquakes (4) in Changning, Sichuan, China (M_s 6.0, 17 June 2019); Laos (M_s 6.0, 21 November 2019); Jiashi, Xinjiang (M_s 6.4, 19 January 2020); and Tajikistan (M_s 6.1, 13 February 2021) were preceded only by anomalies in electron density, whereas the other five were preceded by anomalies in both electron and oxygen ion density (Figures 2 and 3). Furthermore, 78.6% (11/14) of the anomalies occurred within one week before its corresponding earthquake and the other 21.4% (3/14) occurred within two weeks before. The anomalous electron and oxygen ion densities ranged from 1.1×10^{10} to $4.5 \times 10^{10}/\text{m}^3$ and from 2.8×10^{10} to $6.0 \times 10^{10}/\text{m}^3$, respectively (Table 1).

The fault type of earthquakes can usually be divided into three types: normal, thrust, and strike-slip. The normal and thrust types of earthquakes are caused by the horizontal tensile and extrusion stresses in the crust, respectively, while the strike-slip earthquake is derived from the horizontal shear stress. In regard to the fault type, only two of the twelve earthquakes were normal fault earthquakes, and most were either thrust (5) or strike-slip (5) earthquakes. In addition, no ionospheric anomalies were detected before the two normal fault earthquakes; therefore, they accounted for 0% of the 9 earthquakes preceded by ionospheric anomalies. In contrast, four of the five thrust earthquakes and all five strike-slip earthquakes were associated with pre-seismic ionospheric anomalies (Figures 1 and 4, Table 1). Thus, ionospheric anomalies were detected before 90% of the thrust and strike-slip earthquakes, which accounted for 44% (4/9) and 56% (5/9) of the anomaly-associated earthquakes, respectively. It is clear that the observation of pre-seismic ionospheric anomalies correlates well with the fault type of earthquakes.

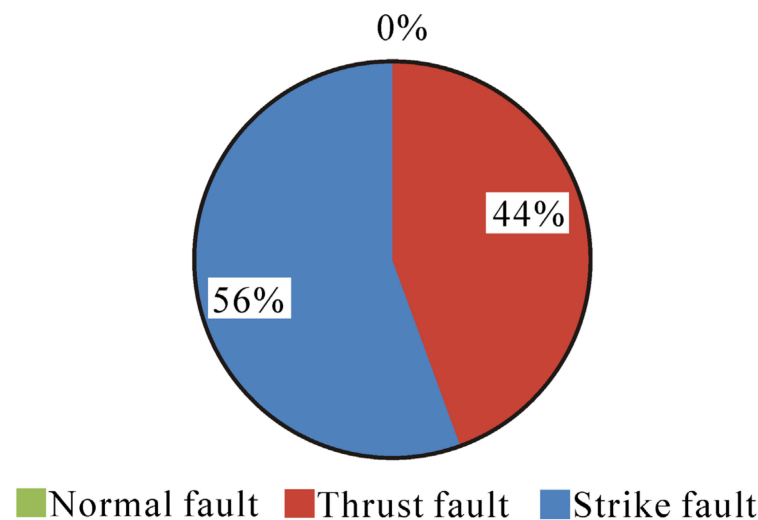


Figure 4. Distribution of anomaly-associated earthquakes among different fault types.

In regard to earthquake location, all three earthquakes that were not preceded by ionospheric anomalies were located within the Tibetan Plateau (Figure 1), whereas the other nine earthquakes preceded by ionospheric anomalies were located on the southeastern and northwestern edges of the Tibetan Plateau. This was consistent with the observations that most normal, strike-slip, and thrust earthquakes occur within the Tibetan Plateau, on the southeastern edge of the Tibetan Plateau, and on the northwestern edge of the Tibetan Plateau, respectively.

3.2. Generation of Anomalous Observations

On 21 May 2021, a 6.4-magnitude earthquake occurred in Yangbi County, Yunnan Province, China and was associated with notable pre-seismic anomalies in both electron and oxygen ion density [32]. In the present study, the Yangbi earthquake was used as a case study to evaluate the mechanisms underlying the generation of electron and oxygen ion density anomalies.

According to the epicenter location of the earthquake, we selected the part closest to the epicenter in the nearest orbit to calculate the ionospheric time sequence (such as the red orbit section in Figure 5). We then calculated the average values of electron density and oxygen ion density of each orbit passing through this position. There are 14 electromagnetic satellite orbits passing through this position during the period of 22–26 May, so we can get the average values of 14 electron densities and oxygen ion densities, respectively. Since the revisit period of the electromagnetic satellite was five days, the time interval for each mean electron and oxygen ion density of the local orbit was five days (Figure 6a,b).

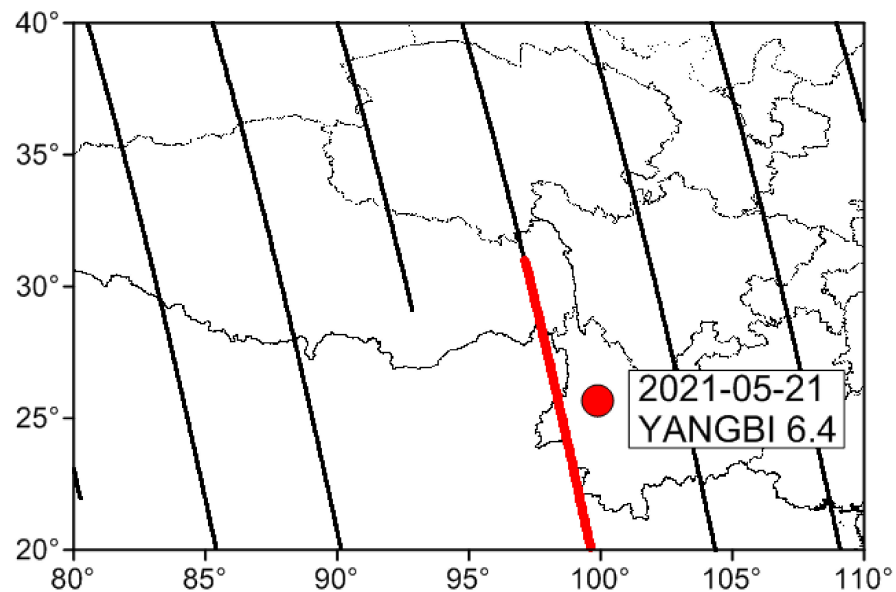


Figure 5. The selection part of orbit used for calculation of ionospheric time sequence. Red circle represents the location of Yangbi Ms 6.4 earthquake.

As shown in Figure 6a, the electron density values fluctuated around $1 \times 10^{10}/\text{m}^3$ from March 22 to May 11, with the highest value of $3.2 \times 10^{10}/\text{m}^3$ on May 16. In Figure 6b, the temporal evolution of oxygen ion density is the same as the electron density, which fluctuated around $1 \times 10^{10}/\text{m}^3$, with the highest value being $4.8 \times 10^{10}/\text{m}^3$. As well, after the Yangbi earthquake (21 May), both the electron and oxygen ion densities decreased significantly.

In order to test the relationship between the earthquakes and ionospheric anomalies, we plotted the frequency of full-magnitude ($M_L \geq 0.9$) earthquakes that occurred within 200 km of the Yangbi earthquake epicenter from March 22 to May 26 (Figure 6c). The results show that the minor earthquake activity increased gradually from May 13 and gradually decreased after the mainshock, which is basically consistent with the evolution of electron density and oxygen ion density anomalies.

The rapid increase of small earthquakes may imply the high stress state of the lithospheric medium. Here, we apply the load/unload response ratio (LURR) method to verify this hypothesis [33–35]. The value of LURR (Y) quantifies the stress state of a non-linear system and is calculated as follows:

$$Y = \frac{X_+}{X_-} \quad (1)$$

where X subscripts “+” and “−” indicate loading and unloading, respectively, and response rate X is defined as:

$$X = \lim_{\Delta P \rightarrow 0} \frac{\Delta R}{\Delta P} \quad (2)$$

where ΔR and ΔP denote changes in payload P and response R when the payload is P .

Furthermore, the LURR based on seismic energy E is defined as follow:

$$Y_m = \left(\sum_{i=1}^{N^+} E_i^m \right)_+ / \left(\sum_{i=1}^{N^-} E_i^m \right)_- \quad (3)$$

where E_i denotes the energy of the i th seismic event, and “+” and “-” denote loading and unloading, respectively. In addition, $m = 1/2$, with E^m denoting the Benioff strain.

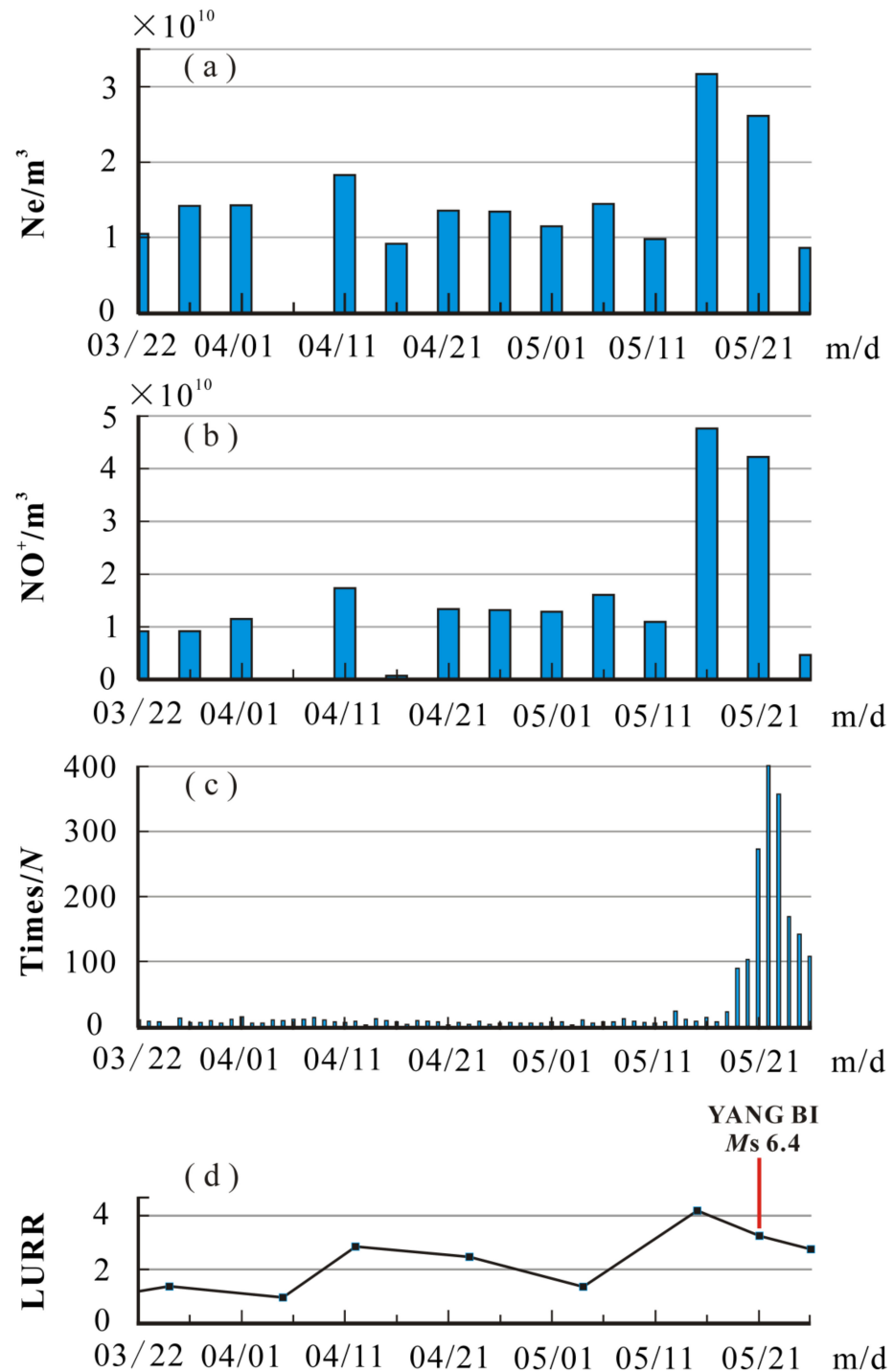


Figure 6. Development of ionospheric anomalies in the two months preceding the 6.4-magnitude earthquake in Yangbi County, Yunnan Province, China. (a) electron density; (b) oxygen ion density; (c) seismic frequency; (d) load/unload response ratio.

As shown in Figure 7, P and R correspond to the load and response of a mechanical system. The response is linear to the load and unload when the load is well below the strength of the system and becomes non-linear when the load reaches a high level, as well as when the system is close to failure [35,36].

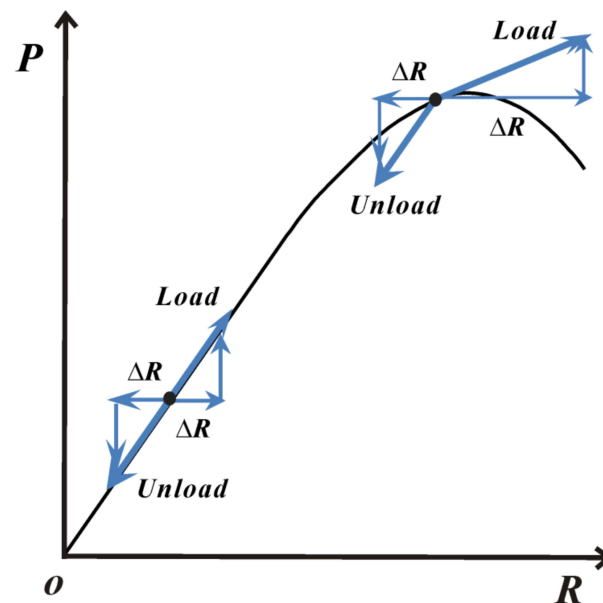


Figure 7. Constitutive relationship of the rock media.

The Benioff strain ($m = 1/2$) of M_L 0–4.9 earthquakes was selected as the response energy within 200 km of the epicenter, from 1 March 2021 to 30 June 2021, and the earthquake source mechanism was taken from the Global Centroid Moment Tensor Project (globalcmt.org) accessed on 1 January 2022, with trend = 46, dip = 78, sliding angle = 4, and depth = 15 km. The friction coefficient within the fault was set as 0.4 and a sliding window of 15 days was used, with a step of 10 days to calculate the LURR value near the epicenter (Figure 6d).

The LURR values gradually increased from March 22 and reached the maximum peak on May 15 (Figure 6d) when the pre-seismic ionospheric anomalies take place, which indicated the high stress state of the source media.

It is clear that before the occurrence of the Yangbi M_S 6.4 earthquake, the electron density, oxygen ion density, and seismic activity augment significantly during the same time period when the stress accumulation in the source media is at a high level, which could be verified by the maximum peak in the LURR time series.

4. Discussion

Lithosphere–atmosphere–ionosphere coupling (LAIC) is the most common explanation for the earthquake-induced ionospheric anomalies. Presently, the explanation of the LAIC mechanism is mainly divided into two categories: the acoustic gravity waves (AGWs) and the electric field [37].

Enhanced seismicity before large earthquakes is a common anomaly. For example, enhanced seismicity was observed near the epicenters of the 2004 Sumatra earthquake (M_W 9.0) in Indonesia, 2010 Yushu earthquake (M_S 7.1), and 2020 Yutian earthquake (M_S 6.4) [38,39]. Previous studies have reported that earthquakes can generate and radiate low-frequency pressure waves [40–42], including infrasound and acoustic-gravity waves, through the sudden vertical undulation and tilting of ground surfaces near the earthquake epicenter [43]. In fact, infrasound anomalies have been observed before the 8.0-magnitude Wenchuan earthquake in 2008, 7.1-magnitude Yushu earthquake in 2010, 9.0-magnitude Japanese earthquake in 2011, and 6.4-magnitude Yangbi earthquake in 2021, with all

infrasound anomalies exhibiting similar amplitude, spectrum, duration, and time from anomaly onset to earthquake [44–47]. A study of “slow earthquakes” reported that slow changes in ground surface can also occur before a large earthquake [48] and that variations in airflow and wind speed resulting from the slow shaking of mountains can produce acoustic-gravity waves [49]. Due to their low frequency, acoustic-gravity waves are only weakly attenuated by the atmosphere, leading to long-range propagation [50], and if such waves are transmitted upward and reach the ionosphere, oscillations in the ionospheric electron and ion densities can occur, thereby producing ionospheric anomalies.

There is another explanation for the mechanism of ionospheric anomalies. During earthquake preparation, with an increase of tectonic stress, the enhancement of fractures induced complex physical and chemical reactions in the crust. In this stage, a large number of additional ions may be yielded. These ions gather at the bottom of the atmosphere, which not only changes the conductivity of the atmosphere but also produces an anomalous surface atmospheric electrostatic field. This electrostatic field may penetrate into the ionospheric height, resulting in the ionospheric anomalies.

By combining with the seismic activity before the Yangbi M 6.4 earthquake, we considered that the pre-seismic ionospheric anomalies were derived from the LAIC acoustic-gravity wave mechanism. Analysis of the Yangbi earthquake indicated that the LURR near the earthquake epicenter continued to increase during the two months before the earthquake (Figure 6d) and during the dilatant stage, which indicated that the material in the seismogenic zone was close to a critical state [51,52]. In addition, minor seismic activity near the earthquake epicenter increased gradually before the earthquake (Figure 5c) and crustal stress near the earthquake epicenter increased constantly, peaking when the material in the seismogenic zone was in the sub-instability stage [51,52]. Furthermore, ground motion increased with crustal stress increases and anomalous sound waves were detected near the earthquake epicenter in mid to early May [38], which indicated that acoustic-gravity waves could have been generated and propagated upward to the ionosphere, resulting in anomalously ionospheric electron and oxygen ion densities. The occurrence of ionospheric anomalies before strong earthquakes could thus be summarized as follows: increased crustal stress in the seismogenic zone caused enhanced ground shaking that generated acoustic-gravity waves, which propagated upward and promoted ionospheric anomalies.

5. Conclusions

The present study investigated the occurrence of ionospheric anomalies before strong earthquakes in and around mainland China and evaluated the potential mechanisms underlying anomaly generation. In most cases, both electron and oxygen ion density anomalies occurred before strong earthquakes in and around western mainland China, and anomalies were strongly associated with thrust and strike-slip earthquakes but not with normal fault earthquakes. Ionospheric anomalies were generated by clear physical mechanisms, including acoustic-gravity waves, which were generated by ground movements and could propagate upward where they promoted anomalous ionospheric perturbations. In regard to earthquake prediction, the combined analysis of ionospheric anomalies and other anomalies or tectonic stress, historical earthquake conditions, or spatial anomaly distribution characteristics can be used to make judgments regarding potential earthquakes.

Author Contributions: Conceptualization, B.Z. and H.Y.; methodology, H.Y.; software, C.Q.; validation, B.Z., N.M. and J.L.; formal analysis, H.Y.; investigation, B.Z.; resources, J.L., C.Y., Y.M. and X.Z.; data curation, B.Z.; writing—original draft preparation, B.Z.; writing—review and editing, H.Y.; visualization, B.Z. and H.Y.; supervision, C.Q.; funding acquisition, H.Y. and B.Z. All authors have read and agreed to the published version of the manuscript.

Funding: Supported by the Earthquake Joint Fund of the National Natural Science Foundation of China (U2039205), National Key Research and Development Program of China (2018YFE0109700), Open Fund for Earthquake Prediction (2021EF0F08), Natural Science Foundation of Xinjiang Uygur Autonomous Region (2021D01A132), and Xinjiang Earthquake Science Foundation (202102).

Institutional Review Board Statement: Not applicable.

Informed Consent Statement: Not applicable.

Data Availability Statement: The data presented in this study are available at <https://www.leos.ac.cn/>.

Conflicts of Interest: The authors declare no conflict of interest.

References

- Li, M.; Wang, F.R.; Zhang, X.D.; Tan, H.D.; Kang, C.L.; Xie, T. Time-spatial statistical characteristics of seismic influence on ionosphere. *Prog. Geophys.* **2014**, *29*, 498–504. (In Chinese)
- Zhang, X.M.; Shen, X.H.; Qian, J.D.; Lu, L.; Chen, H.R.; Ou Yang, X.Y. Advances in the analysis and application of Seismo-electromagnetic Satellite Date in China. *Earthquake* **2009**, *29*, 34–45.
- Hayakawa, M.; Molchanov, O.A. Seismo-Electromagnetics: As a New Field of Radiophysics: Electromagnetic Phenomena Associated with Earthquakes. *URSI Radio Sci. Bull.* **2007**, *2007*, 8–17.
- Hayakawa, M.; Hobara, Y. Current status of electromagnetics for short-term earthquake prediction. *Geomat. Nat. Hazards Risk* **2010**, *1*, 115–155. [[CrossRef](#)]
- Hayakawa, M.; Molchanov, O.A. *Seismo-Electromagnetics: Lithosphere-Atmosphere-Ionosphere Coupling*; Terra Scientific Publishing: Tokyo, Japan, 2002.
- Liu, J.Y.; Chen, Y.I.; Pulinets, S.A.; Tsai, Y.B.; Chuo, Y.J. Seismo-ionospheric signatures prior to $M \geq 6$ Taiwan earthquakes. *Geophys. Res. Lett.* **2000**, *27*, 3113–3116. [[CrossRef](#)]
- Chuo, Y.J.; Liu, J.Y.; Pulinets, S.A.; Chen, Y.I. The ionospheric perturbations prior to the Chi-Chi and Chia-Yi earthquakes. *J. Geodyn.* **2002**, *33*, 509–517. [[CrossRef](#)]
- Singh, R.P.; Singh, B.; Mishra, P.K.; Haykawa, M. On the lithosphere atmosphere coupling of seismo-electromagnetic signals. *Radio Sci.* **2003**, *38*, 1065. [[CrossRef](#)]
- Hayakawa, M.; Horie, T.; Yoshida, M.; Kasahara, Y.; Muto, F.; Ohta, K.; Nakamura, T. On the ionospheric perturbation associated with the 2007 Niigata Chuetsu-oki earthquake, as seen from subionospheric VLF/LF network observations. *Nat. Hazards Earth Syst. Sci.* **2008**, *8*, 573–576. [[CrossRef](#)]
- Akhoondzadeh, M.; Parrot, M.; Saradjian, M.R. Electron and ion density variations before strong earthquakes ($M > 6.0$) using DEMETER and GPS data. *Nat. Hazards Earth Syst. Sci.* **2010**, *10*, 7–18. [[CrossRef](#)]
- Kon, S.; Nishihashi, M.; Hattori, K. Ionospheric anomalies possibly associated with $M \geq 6.0$ earthquakes in the Japan area during 1998–2010: Case studies and statistical study. *J. Asian Earth Sci.* **2011**, *41*, 410–420. [[CrossRef](#)]
- Sorokin, V.M.; Hayakawa, M. On the generation of narrow-banded ULF/ELF pulsations in the lower ionospheric conducting layer. *J. Geophys. Res.* **2008**, *113*, A06306. [[CrossRef](#)]
- Nickolaenko, P.A.; Galuk, P.Y.; Hayakawa, M. The effect of a compact ionosphere disturbance over the earthquake: A focus on Schumann resonance. *Int. J. Appl. Sci.* **2018**, *5*, 11–39. [[CrossRef](#)]
- Pulinets, S.; Boyarsschuc, K. *Ionospheric Precursors of Earthquakes*; Springer Science & Business Media: Berlin/Heidelberg, Germany, 2004.
- Schvets, A.V.; Hayakawa, M.; Molchanov, O.A.; Ando, Y. A study of ionospheric response to regional seismic activity by VLF radio sounding. *Phys. Chem. Earth* **2004**, *29*, 627–637. [[CrossRef](#)]
- Hayakawa, M.; Ohta, K.; Sorokin, V.M.; Yaschenko, J.; Izutsu, J.; Hobara, Y.; Nickolaenko, A.P. Interpretation in terms of gyroscopic waves of Schumann-response-like line emissions observed at Nakatsugawa in possible association with nearby Japanese earthquakes. *J. Atmos. Sol. Terr. Phys.* **2010**, *72*, 1292–1298. [[CrossRef](#)]
- Zhang, X.M.; Shen, X.H.; Ou Yang, X.Y.; Cai, J.A.; Huang, J.P.; Liu, J.; Zhao, S.F. Ionosphere VLF electric field anomalies before Wenchuan M 8 earthquake. *Chin. J. Radio Sci.* **2009**, *24*, 1024–1032.
- Wang, X.Y.; Yang, D.H.; Zhou, Z.H.; Cui, J.; Zhou, N.; Shen, X.H. Features of topside ionospheric background over China and its adjacent areas obtained by the ZH-1 satellite. *Chin. J. Geophys.* **2021**, *64*, 391–409. (In Chinese)
- Ceng, Z.H.; Zhang, B.; Fang, G.Y.; Wang, D.F.; Yin, H.J. The analysis of ionospheric variations before Wenchuan earthquake with DEMETER date. *Chin. J. Geophys.* **2009**, *52*, 11–19. (In Chinese)
- Yan, R.; Wang, L.W.; Hu, Z.; Liu, D.P.; Zhang, X.G.; Zhang, Y. Ionospheric disturbances before and after strong earthquakes based on DEMETER data. *Acta Seismol. Sin.* **2013**, *35*, 498–511.
- Liu, J.; Wan, W.X.; Huang, J.P.; Zhang, X.M.; Zhao, S.F.; Ou Yang, X.Y.; Ze Ren, Z.M. Electron density perturbation before Chile M8.8 earthquake. *Chin. J. Geophys.* **2011**, *54*, 2717–2725. (In Chinese)
- Zhang, Z.X.; Li, X.Q.; Wu, S.G.; Ma, Y.Q.; Shen, X.H.; Chen, H.R.; Wang, P.; You, X.Z.; Yuan, Y.H. DEMETER satellite observations of energetic particle prior to Chile earthquake. *Chin. J. Geophys.* **2012**, *55*, 1581–1590. (In Chinese)
- Zhang, X.M.; Liu, J.; Shen, X.H.; Parrot, M.; Qian, J.D.; Ou Yang, X.Y.; Zhao, S.F.; Huang, J.P. Ionospheric perturbations associated with the M8.6 Sumatra earthquake on 28 March 2005. *Chin. J. Geophys.* **2010**, *53*, 567–575. (In Chinese)
- Zhang, X.M.; Liu, J.; Qian, J.D.; Shen, X.H.; Cai, J.A.; Ou Yang, X.Y.; Zhao, S.F. Ionospheric electromagnetic disturbance before Gaize earthquake with MS6.9, Tibet. *Earthquake* **2008**, *28*, 14–22.

25. Zhang, X.M.; Qian, J.D.; Ou Yang, X.Y.; Cai, J.A.; Liu, J.; Shen, X.H.; Zhao, S.F. Ionospheric electro-magnetic disturbances prior to Yutian 7.2 earthquake in Xinjiang. *Chin. J. Space Sci.* **2009**, *29*, 213–221.
26. Wang, X.Y.; Cheng, W.L.; Yang, D.H.; Liu, D.P. Preliminary validation of in situ electron density measurements onboard CSES using observations from Swarm Satellites. *Adv. Space Res.* **2019**, *64*, 982–994. [[CrossRef](#)]
27. Shen, X.H.; Zhang, X.M.; Yuan, S.G.; Wang, L.W.; Cao, J.B.; Huang, J.P.; Zhu, X.P.; Piergiorgio, P.; Dai, J.P. The state-of-the-art of the China Seismo-Electromagnetic Satellite mission. *Sci. China Technol. Sci.* **2018**, *61*, 634–642. [[CrossRef](#)]
28. Yan, R.; Shen, X.H.; Huang, J.P.; Wang, Q.; Chu, W.; Liu, D.P.; Yang, Y.Y.; Lu, H.X.; Xu, S. Examples of unusual ionospheric observations by the CSES prior to earthquakes. *Earth Planet. Phys.* **2018**, *2*, 515–526. [[CrossRef](#)]
29. Deng, Q.D.; Zhang, P.Z.; Ran, K.Y.; Yang, X.P.; Min, W.; Chu, Q.Z. Basic features of active tectonics in China. *Sci. China (Ser. D)* **2002**, *32*, 1020–1030.
30. Xu, Z.Q.; Yang, J.S.; Li, H.B.; Ji, S.C.; Zhang, Z.M.; Liu, Y. One the tectonics of the India-Asia collision. *Acta Geol. Sin.* **2011**, *85*, 1–33.
31. Deng, Q.D.; Cheng, S.P.; Ma, Y.; Du, P. Seismic activities and earthquake potential in the Tibetan Plateau. *Chin. J. Geophys.* **2014**, *57*, 2025–2042. (In Chinese)
32. Wang, G.M.; Wu, Z.H.; Peng, G.L.; Liu, Z.F.; Luo, R.J.; Huang, X.L.; Chen, H.P. Seismogenic fault and it's rupture characteristics of the 21 May 2021 Yangbi MS 6.4 earthquake, analysis results from the relocation of the earthquake sequence. *J. Geomech.* **2021**, *27*, 662–678.
33. Yin, X.C.; Yin, C. The Precursor of Instability for Nonlinear System and its Application to Earthquake Prediction. *Sci. China* **1991**, *34*, 977–986.
34. Yin, X.C.; Chen, X.Z.; Song, Z.P.; Yin, C. A New Approach to Earthquake Prediction-The Load Unload Response Ratio (LURR) Theory. *Pure Appl. Geophys.* **1995**, *145*, 701–715. [[CrossRef](#)]
35. Yin, X.C.; Wang, Y.C.; Peng, K.Y.; Bai, Y.L.; Wang, H.T.; Yin, X.F. Development of a new approach to earthquake prediction: Load/unload response ratio (LURR) theory. *Pure Appl. Geophys.* **2000**, *157*, 2365–2383. [[CrossRef](#)]
36. Yu, H.Z.; Zhu, Q.Y. A probabilistic approach for earthquake potential evaluation based on the load/unload response ratio method. *Concurr. Comput. Pract. Exp.* **2010**, *22*, 1520–1533. [[CrossRef](#)]
37. Yang, X.B. Study of Lithosphere-Atmosphere-Ionosphere Electric Field Coupling. Ph.D. Thesis, Wuhan University, Wuhan, China, 2015.
38. Chen, X.Z.; Li, Y.E. Distribution characteristics of the month-scale and week-scale numbers for small earthquakes around the epicenter prior to the 14 April 2010 Yushu earthquake with MS7.1. *Earthq. Res. China* **2012**, *28*, 10–21.
39. Chen, X.Z.; Li, Y.E.; Wang, H.X.; Guo, X.Y. The enhancement of seismicity before the 2004 MW 9.0 Indonesia Sumatra earthquake and its relation to the earth rotation. *Chin. J. Geophys.* **2013**, *56*, 79–90. (In Chinese)
40. Bolt, B.A. Seismic air waves from the great 1964 Alaskan earthquake. *Nature* **1964**, *202*, 1095–1096. [[CrossRef](#)]
41. Shinagawa, H.; Iyemori, T.; Saito, S.; Maruyama, T. A numerical simulation of ionospheric and atmospheric variations associated with the Sumatra earthquake on 26 December 2004. *Earth Planets Space* **2007**, *59*, 1015–1026. [[CrossRef](#)]
42. Mikumo, T.; Shibutani, T.; Le Pichon, A.; Garces, M.; Fee, D.; Tsuyuki, T.; Watada, S.; Morii, W. Low-frequency acoustic-gravity waves from coseismic vertical deformation associated with the 2004 Sumatra-Andaman earthquake (MW = 9.2). *J. Geophys. Res.* **2008**, *113*, B12402. [[CrossRef](#)]
43. Mutschlecner, J.P.; Whitaker, R.W. Infrasound from earthquakes. *Geophys. Res.* **2005**, *110*, D0108. [[CrossRef](#)]
44. Lin, L.; Yang, Y.C. Observation and study of a kind of low-frequency atmospheric infrasonic waves. *Acta Acust.* **2010**, *35*, 200–207.
45. Xia, Y.Q.; Cui, X.Y.; Li, J.Z.; Chen, W.S.; Liu, C.Y. Research of abnormal infrasound signals before worldwide earthquakes. *J. Beijing Univ. Technol.* **2011**, *37*, 463–469.
46. Yang, Y.C.; Guo, Q.; Lv, J.; Teng, X.P. Observation and study of precursor infrasound waves emitted before several strong earthquakes. *Acta Phys. Sin.* **2014**, *63*, 134302. [[CrossRef](#)]
47. Guo, Q.; Yang, X.H.; Liu, S.S. Infrasound anomaly analysis and background spatial distribution characteristics before Yangbi M6.4 earthquake. Abstract of the paper. In Proceedings of the 2021 Annual Meeting of Seismic Fluid Committee, Seismological Society of China, Online, 19–23 April 2021.
48. Chen, S.G.; Yang, F.; Chen, J.F.; Yan, W.S.; Tian, W.T. Characteristics of Long-Period Deformation Wave. *J. Seismol. Res.* **2011**, *34*, 308–312.
49. Lv, J.; Yang, Y.C.; Feng, H.N.; Chunchuzov, I.; Teng, P.X. Study on generation mechanism of anomalous acoustic-gravity waves before the 2011 Beijing earthquake (ML = 3.0). *Acta Acust.* **2015**, *40*, 307–316.
50. Le Pichon, A.; Blanc, E.; Hauchecorne, A. *Infrasound Monitoring for Atmospheric Studies*; Springer: New York, NY, USA, 2010; p. 7.
51. Scholz, C.H.; Sykes, L.R.; Aggarwal, Y.P. Earthquake prediction: A physical basis. *Science* **1973**, *181*, 803–809. [[CrossRef](#)]
52. Ma, J.; Sherman, S.I.; Guo, Y.S. Identification of meta-unstable stress state based on experimental study of evolution of the temperature field during stick-slip instability on a 5° bending fault. *Sci. China Earth Sci.* **2012**, *55*, 869–881.